



HAL
open science

Simultaneous collision-induced transitions in H₂O+CO₂ gas mixtures

H. Fleurbaey, D. Mondelain, W. Fakhardji, J.M. Hartmann, A. Campargue

► **To cite this version:**

H. Fleurbaey, D. Mondelain, W. Fakhardji, J.M. Hartmann, A. Campargue. Simultaneous collision-induced transitions in H₂O+CO₂ gas mixtures. *Journal of Quantitative Spectroscopy and Radiative Transfer*, 2022, 285, pp.108162. 10.1016/j.jqsrt.2022.108162 . hal-03865599

HAL Id: hal-03865599

<https://hal.science/hal-03865599>

Submitted on 22 Nov 2022

HAL is a multi-disciplinary open access archive for the deposit and dissemination of scientific research documents, whether they are published or not. The documents may come from teaching and research institutions in France or abroad, or from public or private research centers.

L'archive ouverte pluridisciplinaire **HAL**, est destinée au dépôt et à la diffusion de documents scientifiques de niveau recherche, publiés ou non, émanant des établissements d'enseignement et de recherche français ou étrangers, des laboratoires publics ou privés.

1
2
3
4
5
6
7
8
9
10
11
12
13
14
15
16
17
18
19
20
21
22
23
24
25
26
27
28

Simultaneous collision-induced transitions in H₂O+CO₂ gas mixtures

H. Fleurbaey^a, D. Mondelain^a, W. Fakhardji^b, J.-M. Hartmann^b, A. Campargue^{a*}

^a *Univ. Grenoble Alpes, CNRS, LIPhy, 38000 Grenoble, France*

^b *Laboratoire de Météorologie Dynamique/IPSL, CNRS, Ecole Polytechnique, Institut polytechnique de Paris, Sorbonne Université, Ecole Normale Supérieure, PSL Research University, F-91120 Palaiseau, France*

Key words

Absorption spectroscopy; Radiative transfer; Collision Induced Absorption; Continuum

* Corresponding author: alain.campargue@univ-grenoble-alpes.fr; LIPhy, Bat. E, 140 rue de la Physique, 38400 Saint-Martin d'Hères (France).

29

Abstract

30 A collision induced absorption (CIA) band has been measured near 6000 cm^{-1} in a spectrum of
31 humidified CO_2 recorded by cavity ring down spectroscopy (CRDS) at low pressure ($<1\text{ atm}$). This
32 absorption adds a contribution to the $\text{H}_2\text{O}+\text{CO}_2$ continuum mostly originating from far wings of the CO_2
33 and H_2O resonance lines broadened by collisions with H_2O and with CO_2 , respectively. The observed
34 CIA corresponds to a simultaneous excitation of $^{12}\text{CO}_2$ and H_2O colliding molecules in the ν_3
35 antisymmetric and ν_1 symmetric stretching mode, respectively. CRDS spectra recorded near 5940 cm^{-1}
36 with a highly enriched $^{13}\text{CO}_2$ sample provide a confirmation of the assignment since the measured
37 CIA isotopic spectral shift (of about -68 cm^{-1}) coincides with that between the ν_3 bands of $^{12}\text{CO}_2$ and
38 $^{13}\text{CO}_2$. The integrated binary coefficient of the two CIA is evaluated and found to be on the order of
39 $2.3\times 10^{-3}\text{ cm}^{-2}\text{ amagat}^{-2}$. Classical molecular dynamics simulations (CMDS) of the considered CIA are also
40 presented, based on the dominant dipole induction mechanism associated with the vibrational matrix
41 elements of the dipole of CO_2 (ν_3) and isotropic polarizability of H_2O (ν_1). The results of the calculations
42 are found in good agreement with the observations, thus further validating the attribution of the
43 observed CIA structure to the above mentioned double transitions.

44

45 **I. Introduction**

46 The absorption of light by pure water vapor involves two contributions. The first one is the
47 monomolecular absorption due to the rovibrational resonance lines which is proportional to the water
48 vapor pressure. The second one, varying smoothly with the frequency, is the so-called water vapor
49 self-continuum, which is proportional to the squared molecular density as it is due to interactions
50 between pairs of water molecules. There are three potential contributions to this continuum, which
51 include the far wings of the resonance lines, collision-induced absorption (CIA) by interacting pairs of
52 free (unbound) molecules, and dimers (note that the latter may be considered as a part of the CIA
53 since they also involve the dipole of a pair of molecules, even though in many cases they negligibly
54 contribute to it). Similarly, the absorption spectrum of pure carbon dioxide involves resonance lines
55 and a self-continuum contribution again resulting from the three contributions mentioned above
56 generating absorptions proportional to the squared gas density. Numerous experimental and
57 theoretical studies have been devoted to the self-continua of both H₂O and CO₂ (see [1] and chapters
58 V and VI of [2]) due to their importance for radiative transfer processes in the atmospheres of the Earth
59 and Venus, respectively.

60 However, the self-continua are not the only continua relevant for planetary applications. Since
61 planetary atmospheres are mixtures of various molecular species, there are additional “crossed”
62 absorption contributions, proportional to the product of the densities of the different colliding
63 molecules. This leads to non-additive absorption as for example in the Earth atmosphere in which the
64 H₂O- and CO₂-air (or N₂) continua play, together with the H₂O self-continuum, a significant role which
65 has motivated a large number of studies (see [1] and chapters V and VI of [2]). Note that, until recently,
66 it was generally considered that the associated atmospheric continua were essentially due to the far
67 wings of the air-broadened lines of H₂O and CO₂. The recent demonstration of the importance of an
68 N₂ absorption band induced by collisions with H₂O in the H₂O-N₂ continuum [3,4] pointed out the limits
69 of this assumption.

70 Due to its potential importance for the atmospheres of Early Mars and exoplanets, the
71 continuum in H₂O-CO₂ mixtures has recently received a renewed attention, nearly 30 years after
72 pioneer studies devoted to the CO₂-broadened line wings of H₂O for Venusian studies [5,6].
73 Measurements and calculations have been made in order to characterize the influence of collisions
74 with H₂O on the wings of CO₂ lines [3,7,8] as well as that of collisions with CO₂ on the wings of H₂O
75 lines [7,9]. It is worth mentioning that the importance of non-additivity effects in absorption in
76 H₂O+CO₂ mixtures (in particular, those related to weak simultaneous transitions – see below) was first
77 discussed by Vigasin et al. in 1994, on the basis of infrared absorption spectra of moisture-containing
78 CO₂ in the liquid and gaseous phases [10].

79 Very recently, we have undertaken a series of measurements aiming to characterize the
80 absorption continuum of H₂O-CO₂ mixtures in the 1.6 μm and 2.3 μm windows and near 3.5 μm,
81 corresponding to low opacity regions for both CO₂ and water vapor [11]. The “crossed” absorption
82 (proportional to the product of the H₂O and CO₂ densities) was observed to include an unexpected
83 broad band, centered near 6000 cm⁻¹, in addition to the contributions of the far wings of the lines of
84 the monomers (note that pure CO₂ spectra do not exhibit any CIA band in this spectral region [12]). On
85 the basis of the spectral position of its center, this band was tentatively assigned to the simultaneous
86 collision-induced transitions involving a ν_1 (Raman) excitation of H₂O and a ν_3 (dipole absorption)
87 excitation of ¹²CO₂ [noted $\nu_3(\text{CO}_2)+\nu_1(\text{H}_2\text{O})$, hereafter] but no further analysis was made. Note that such
88 simultaneous transitions (sometimes also denoted as double transitions), resulting from the
89 polarization of one molecule (*e.g.* through a vibrational matrix element of the polarizability) by the
90 vibrating electric field of the collision partner (*e.g.* through a vibrational matrix element of the electric
91 dipole or quadrupole) have been observed (starting in the early 50’s !) and analyzed for diverse
92 molecular systems involving H₂ or N₂ (*e.g.* [13,14,15,16,17]), but also for pure CO₂ [18], CO₂-N₂
93 [19,20,21,22,23] and CO₂-H₂ [24], to cite but a few. Also recall the pioneer work of Colpa and Ketelaar
94 [24] which set the theoretical bases for practical calculations of their integrated intensity.

95 In this paper, we revisit the $\nu_3(\text{CO}_2)+\nu_1(\text{H}_2\text{O})$ CIA band both experimentally, by complementing
96 the natural CO₂ measurements reported in Ref. [11] by a new investigation using ¹³CO₂, and
97 theoretically, by using a simple induction model and molecular dynamics simulations. In the next
98 section, we summarize the conditions of the acquisition of the humidified CO₂ spectra by cavity ring
99 down spectroscopy (CRDS). The different steps of the CIA retrieval by successive subtraction of the
100 different contributions from the measured spectra are also described in this section. In section 3, the
101 classical molecular dynamics simulations (CMDs) and the input data used for the prediction of the CIA
102 are described. The measured and calculated results are then presented and discussed in Sec. 4, before
103 concluding remarks (Sec. 5).

104 **2. CRDS recordings and CIA retrieval**

105 **2.1. Data acquisition**

106 The inherent sensitivity and baseline stability of cavity enhanced techniques make them
107 particularly suitable to measure weak continua [25]. They, in particular, enable to use samples at sub-
108 atmospheric pressure while traditional methods are generally combined with pressurized cells. This is
109 crucial in the case of mixtures involving water vapor at room temperature, the limitation by the
110 saturation pressure making accurate absorption measurements by FTS with long absorption
111 pathlengths practically impossible in the atmospheric transparency windows. In contrast,
112 measurements by CRDS and OFCEAS have recently led to accurate determinations of the self- and

113 foreign (air)-continua of H₂O [26,27,28,29,30,31]. Another advantage of recordings at sub-atm
114 pressures is that the contribution of local absorption transitions is easier to calculate and remove, since
115 line-mixing effects may be disregarded and isolated line shapes can be used. For instance, CRDS was
116 recently applied to the characterization of the O₂ CIA band at 1.27 μm both at NIST [32] and in our
117 laboratory [33,34]. The use of low O₂ pressures enabled to minimize the impact of line mixing effects
118 on the CIA determination obtained with an agreement of less than 1% between the two datasets at
119 room temperature.

120 The $\nu_3(\text{CO}_2)+\nu_1(\text{H}_2\text{O})$ CIA band was observed in CRDS spectra of humidified CO₂ recorded in the
121 5725-6665 cm⁻¹ and 5856-5986 cm⁻¹ intervals, for natural CO₂ and ¹³CO₂ samples, respectively.
122 Distributed feedback (DFB) laser diodes were used as light sources, each of them covering a spectral
123 range 20 to 30 cm⁻¹ wide by temperature variation. The cavity-ring down spectrometer used a 142 cm
124 long high finesse cavity fitted with two highly reflective dielectric mirrors. Ring down (RD) times were
125 of the order of 120 to 160 μs. Typically, ten RD times were averaged at each spectral step separated
126 by 0.005 cm⁻¹. A part of the laser light was sent into a wavelength meter (model 621-A IR from Bristol)
127 to monitor the laser frequency.

128 As detailed in Ref. [11], the spectra with natural CO₂ were recorded in flow regime using
129 H₂O+CO₂ mixtures with H₂O molar fractions between 3000 and 15000 ppmv. The gas flow of the
130 mixture (typically a few tens sccm inside the CRDS cavity) was produced using a commercial humidity
131 generator (from Omicron Technologies). The total pressure in the CRDS cavity was monitored by a
132 sensor from Edwards (1000 mbar full scale, accuracy 0.15 % of reading) and maintained at a fixed value
133 of 400 or 750 Torr with a solenoid valve and a software-based proportional integral loop acting on the
134 gas flow. The densities of CO₂ and H₂O (ρ_{CO_2} and $\rho_{\text{H}_2\text{O}}$, respectively) were obtained from the partial
135 pressures and the cell temperature measured with a calibrated Pt100 sensor (2σ-uncertainty ±0.06°C)
136 fixed on the external wall of the cavity underneath the enveloping thermal insulation foam.

137 In the case of the recordings with humidified ¹³CO₂, the limitation of the gas consumption
138 (imposed by the cost of the ¹³C enriched CO₂ tank) required to record the spectra in static regime. The
139 cell was thus first filled with about 6.5 Torr of water vapor and ¹³CO₂ (from Aldrich, 99 % ¹³C
140 enrichment) was then added up to a total pressure of 400 Torr.

141 The baseline determination of the spectra relied on measurements performed with argon
142 before and after the recording with the (H₂O+CO₂) mixture, with the cavity pumped before each gas
143 filling (argon or mixture). The two argon spectra ensure that the cavity alignment (and thus the
144 baseline) is unchanged after pumping/filling cycles. By comparing the two argon spectra, the baseline
145 stability was found to be of the order of a few 10⁻¹⁰ cm⁻¹. In order to check the proportionality of the
146 retrieved “crossed” absorption to the $\rho_{\text{CO}_2}\rho_{\text{H}_2\text{O}}$ densities product, measurements were performed for
147 several values of the water molar fraction in natural CO₂. The study with ¹³CO₂ being mostly performed

148 for validation of the assignment of the observed CIA structure, a single set of experimental conditions
149 (~6.5 Torr of water vapor in $^{13}\text{CO}_2$ at a total pressure of 400 Torr) was retained.

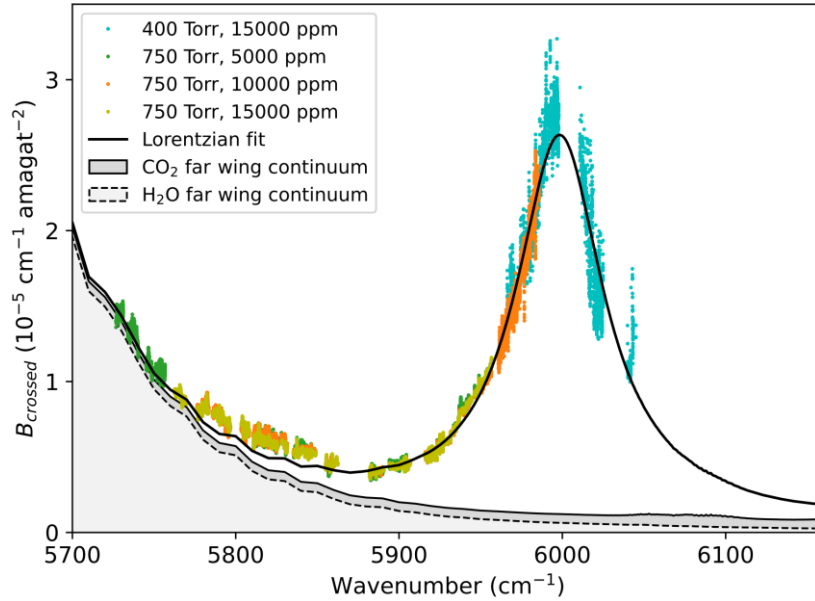
150 2.2. CIA retrieval

151 After baseline correction, the absorption coefficient, $\alpha(\nu)$, can be expressed as:

$$152 \quad \alpha(\nu) = M_{\text{CO}_2}\rho_{\text{CO}_2} + M_{\text{H}_2\text{O}}\rho_{\text{H}_2\text{O}} + B_{\text{CO}_2}\rho_{\text{CO}_2}^2 + B_{\text{H}_2\text{O}}\rho_{\text{H}_2\text{O}}^2 + B_{\text{crossed}}\rho_{\text{CO}_2}\rho_{\text{H}_2\text{O}} \quad (1)$$

153 where $M_{\text{CO}_2}\rho_{\text{CO}_2}$ and $M_{\text{H}_2\text{O}}\rho_{\text{H}_2\text{O}}$ are the contributions due to the monomer local lines of CO_2 and H_2O
154 (calculated within a $\pm 25 \text{ cm}^{-1}$ range around the center wavenumber), respectively, and ρ represents
155 the density (in amagat^{-1}). The $B_{\text{H}_2\text{O}}$ and B_{CO_2} coefficients (in $\text{cm}^{-1}\text{amagat}^{-2}$) correspond to the self-
156 continuum coefficients of water and CO_2 , respectively. B_{crossed} is the crossed binary coefficient arising
157 from the interaction of water and CO_2 molecules, thus involving both far line wings (of CO_2 -broadened
158 H_2O transitions as well as of H_2O -broadened CO_2 transitions) and CIA bands contributions.

159 In the case of natural CO_2 , the HITRAN2016 database [35] was used to simulate the local CO_2
160 and H_2O monomer contributions with Voigt profiles truncated at $\pm 25 \text{ cm}^{-1}$ excluding the pedestal of
161 the absorption lines (see details in Ref. [11]). The water self-continuum cross-sections $B_{\text{H}_2\text{O}}$ were taken
162 from Ref. [30] while, for CO_2 , the self-continuum cross-sections B_{CO_2} were taken from Ref. [12] or
163 measured in Ref. [11] below and above 5800 cm^{-1} , respectively. The B_{crossed} binary coefficients
164 measured with the natural CO_2 sample for various water vapor molar fractions (from 3000 to 15000
165 ppm) and two total pressures (400 and 750 Torr) are presented in **Fig. 1**. While over the various
166 experimental conditions the $\rho_{\text{CO}_2}\rho_{\text{H}_2\text{O}}$ density product varied by a factor of 5, the set of retrieved
167 B_{crossed} values are found consistent within about 20 % in the CIA region near 6000 cm^{-1} . **Fig. 1** also
168 includes a fit of the observed band, assuming a Lorentzian shape and fixing the far wing continuum
169 background to its value calculated by the χ -factor approach (see [11]). The parameters obtained from
170 this Lorentzian fit will be discussed in Sec. 4.

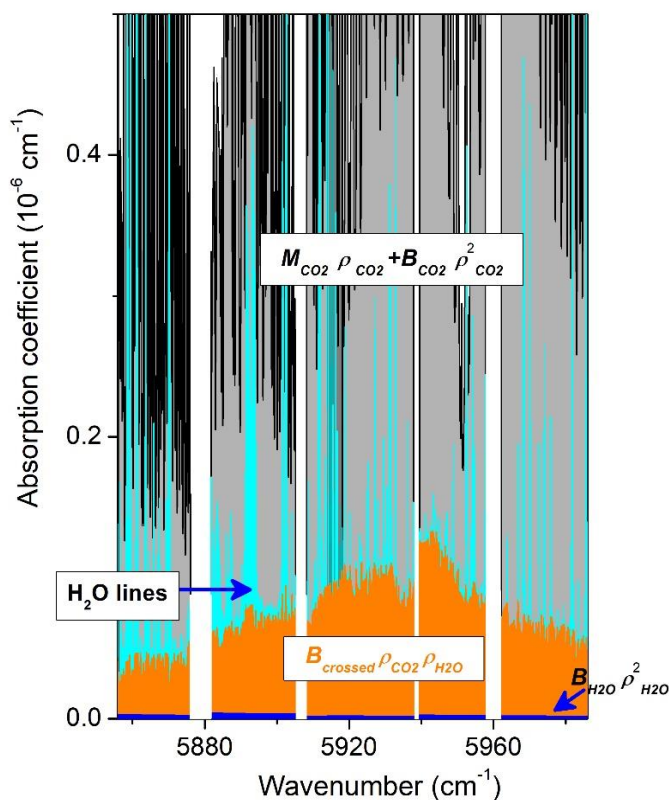


171

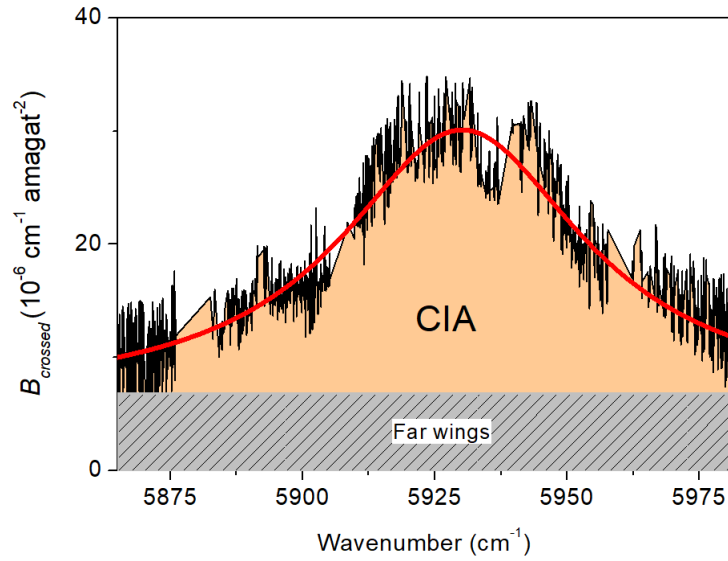
172 **Fig.1:** Overview of the binary coefficients measured in the 5725-6040 cm^{-1} region including the $\nu_3(^{12}\text{CO}_2)+\nu_1(\text{H}_2\text{O})$
 173 CIA band near 6000 cm^{-1} , for various total pressures and water vapor molar fractions. The best fit of the CIA using
 174 a Lorentzian function (black solid line) is superimposed to the far wing continuum background which was fixed to
 175 its value calculated by the χ -factor approach (see [11]).

176 In the case of humidified $^{13}\text{CO}_2$, the measurement of the CIA band is made more difficult because
 177 it falls in a region where CO_2 resonance lines are much stronger than with the natural sample. In order
 178 to subtract the $^{13}\text{CO}_2$ contribution $-(M_{\text{CO}_2}\rho_{\text{CO}_2} + B_{\text{CO}_2}\rho_{\text{CO}_2}^2)$ in Eq. (1) – we did not try to simulate
 179 separate contributions of the resonance lines and of the self-continuum of $^{13}\text{CO}_2$ and preferred to
 180 directly subtract a spectrum of dry $^{13}\text{CO}_2$ recorded at the same partial pressure of $^{13}\text{CO}_2$ as in the
 181 humidified mixture used for the recordings (395 Torr). This, which disregards the effects of collisions
 182 with H_2O on the central and wing regions of the $^{13}\text{CO}_2$ lines, is of likely small consequences considering
 183 the relatively small (1.5 %) amount of water vapor in the humidified sample. **Fig. 2** shows the different
 184 contributions to the total absorption coefficient measured for a mixture of about 6 Torr of water in
 185 $^{13}\text{CO}_2$ at a total pressure of 400 Torr. As adsorption on the walls of the CRDS affected the amount of
 186 water in the cell, for the spectral interval corresponding to the tuning range of each DFB laser diode,
 187 the water vapor partial pressure, $p_{\text{H}_2\text{O}}$, was determined from the integrated absorption coefficient of
 188 a few observed water lines. The obtained $p_{\text{H}_2\text{O}}$ values were found to vary from 5.3 to 7.0 Torr for the
 189 six DFB intervals covering the CIA region (5856-5986 cm^{-1}). These $p_{\text{H}_2\text{O}}$ values were used to calculate
 190 and subtract the water self-continuum [30] and the water resonance lines contribution (computed
 191 using the HITRAN2016 line list [35]). As illustrated by **Fig. 2**, in our experimental conditions, the two
 192 water vapor contributions are much smaller than the $^{13}\text{CO}_2$ contribution. After subtraction of the
 193 different contributions, the remaining absorption coefficient $-B_{\text{crossed}}\rho_{\text{CO}_2}\rho_{\text{H}_2\text{O}}$ shows a clear bell
 194 shape centered at about 5940 cm^{-1} corresponding to the $\nu_3(^{13}\text{CO}_2)+\nu_1(\text{H}_2\text{O})$ CIA band. Using the

195 determined p_{H_2O} values, the corresponding crossed binary coefficients, $B_{crossed}$, displayed in **Fig. 3**
 196 were derived. The obtained curve shows high frequency “noise” due to the imperfect removal of the
 197 strong $^{13}CO_2$ resonance lines. An improved description of the CIA band shape is obtained from a
 198 Lorentzian fit with a baseline (corresponding to the far wing continuum contribution) assumed to be
 199 constant with frequency. The parameters obtained from this fit will be discussed in Sec. 4.
 200



201
 202 **Fig. 2:** Different contributions to the total absorption coefficient measured by CRDS with a mixture of water and
 203 CO_2 highly enriched in ^{13}C . The total pressure was 402 Torr while the water vapor partial pressure varied between
 204 5.3 and 7.0 Torr over the displayed region. The measured absorption coefficient is first reduced by the $^{13}CO_2$
 205 contribution (lines and self-continuum - grey background) measured with a pure $^{13}CO_2$ sample. Then, the water
 206 contribution (lines and self-continuum - cyan and blue background, respectively) is simulated and subtracted. The
 207 absorption remaining after these subtractions (orange background) shows the bell shape profile of the
 208 $\nu_3(^{13}CO_2)+\nu_1(H_2O)$ CIA band centered near 5930 cm^{-1} .



209

210 **Fig 3:** Crossed binary coefficients in the region of the $\nu_3(^{13}\text{CO}_2)+\nu_1(\text{H}_2\text{O})$ CIA band. The best fit of the CIA Lorentzian
 211 shape (red solid line) is superimposed to the continuum background due to the far wing continuum (dashed). The
 212 background level was adjusted by the fit.
 213

214 3. Classical molecular dynamics simulations (CMDS)

215 The CIA in the region of the $\nu_3(\text{CO}_2)+\nu_1(\text{H}_2\text{O})$ simultaneous transitions was calculated using
 216 classical molecular dynamics simulations (CMDS), exactly as described in Ref. [3] for $\text{CO}_2+\text{H}_2\text{O}$, with the
 217 only difference that the H_2O static isotropic polarizability matrix element $\langle v = 0 | \alpha_{iso}(\text{H}_2\text{O}) | v = 0 \rangle$
 218 used in this previous study was here replaced by the vibrational matrix element $\langle v =$
 219 $0 | \alpha_{iso}(\text{H}_2\text{O}) | v_1 = 1 \rangle$ (here, $v = 0$ and $v_1 = 1$ stand for the (000) and (100) vibrational states of H_2O ,
 220 respectively). Since details on the CMDS can be found in Ref. [3] and references cited therein, only the
 221 main elements are recalled here. The simulations start with the initialization, for each molecule, of its
 222 center of mass position (inside a cubic box of dimensions defined by the gas density and total number
 223 of molecules treated) and translational velocity vector, and of its angular orientation and rotational
 224 angular momentum vector. These are set in order to verify the Boltzmann statistics for the considered
 225 temperature. The propagation in time of these four molecular parameters is then computed using the
 226 equations of classical mechanics fed by forces and torques due to intermolecular interactions
 227 computed using the same input site-site $\text{CO}_2\text{-H}_2\text{O}$ as in Ref. [3]. Periodic boundary conditions, nearest
 228 neighbour spheres, the Verlet algorithm, and the quaternions approach [36] were used and about 5
 229 million molecules were treated. After a temporization time of $t_0 = 20$ ps to let the system properly
 230 thermalize, the dipole $\vec{\mu}_{ij}(t)$ induced in ($i=\text{CO}_2, j=\text{H}_2\text{O}$) colliding pairs was computed. As in Ref. [3], only
 231 the component of the induced dipole due to the polarization of H_2O (through its isotropic polarizability
 232 $\langle v = 0 | \alpha_{iso}(\text{H}_2\text{O}) | v_1 = 1 \rangle$) in the electric field of the CO_2 dipole (through $\langle v = 0 | \mu(\text{CO}_2) | v_3 = 1 \rangle$,
 233 where $v = 0$ and $v_3 = 1$ stands for the $(v_1 v_2 l_2 v_3) = (00^0 0)$ and $(00^0 1)$ vibrational states of CO_2 ,

234 respectively) was taken into account. This is convenient since the induced dipole – driven by the
 235 $B_{1012}(R)$ term of Eq. (4.50) of [37] or the first term in Eq. (10) of Ref. [24] – then only depends on the
 236 orientations of the CO₂ axis and of the vector between the centers of mass of the two molecules, and
 237 is independent from the orientation of the H₂O molecule. Note that this disregards other induction
 238 mechanisms, including the term originating from the anisotropic polarizability of the water molecule
 239 (*i.e.* $\langle v = 0 | \Delta\alpha(\text{H}_2\text{O}) | v_1 = 1 \rangle$). However note that, as discussed below, this contribution is likely
 240 relatively small, while many other terms, such as those involving the product of the H₂O dipole element
 241 $\langle v = 0 | \mu(\text{H}_2\text{O}) | v_1 = 1 \rangle$ and of the CO₂ polarizability $\langle v = 0 | \Delta\alpha(\text{CO}_2) \text{ or } \alpha_{iso}(\text{CO}_2) | v_3 = 1 \rangle$, vanish
 242 due to symmetry considerations. As in Ref. [3], we used $\langle v = 0 | \mu(\text{CO}_2) | v_3 = 1 \rangle = 0.13$ a. u. [38, 39].
 243 For H₂O, $\langle v = 0 | \alpha_{iso}(\text{H}_2\text{O}) | v_1 = 1 \rangle = 0.73$ a. u. was obtained, using the convention of Ref. [37], from
 244 the value of α_0^0 provided in Ref. [40] with $\alpha_{iso} = -\alpha_0^0/\sqrt{3}$. With the method and input data described
 245 above, the induced dipole was computed from $t_0 (= 20$ ps) to $t_0 + \Delta t (= 5$ ps) in the course of the CMDS.
 246 Then its autocorrelation function was computed using t_0 as the time origin, averaged over all molecules
 247 and Laplace-Fourier transformed to yield the absorption spectrum [41]. Note that our classical
 248 calculations lead to a CIA structure that is automatically centered at the sum of the origins of the
 249 $\nu_3(^{12}\text{CO}_2)$ and $\nu_1(\text{H}_2\text{O})$ bands, $2349 + 3657 = 6006$ cm⁻¹ for ¹²CO₂, because all the *Q* transitions of the H₂O
 250 ν_1 band, associated with the isotropic polarizability, then have the same imposed wavenumber of 3657
 251 cm⁻¹. This, which leads to a difference of about +6 cm⁻¹ between the positions of the CIA peak in the
 252 calculated and measured spectra, does not correspond to reality since the $(v = 0, J, K_a, K_c) \rightarrow$
 253 $(v_1 = 1, J, K_a, K_c)$ rovibrational transitions are all shifted to the red with respect to the band origin
 254 of 3657 cm⁻¹ and spread over typically 10 cm⁻¹ [35]. In order to correct for this, the bar spectrum of the
 255 true *Q* lines was convoluted by the raw CMDS-predicted CIA, which red-shifts the peak wavenumber
 256 by about -6 cm⁻¹ with respect to 6006 cm⁻¹, leading to a very good agreement with the experimental
 257 findings as discussed below. In the case of ¹³CO₂, CMDS were computed as done for ¹²CO₂, using the
 258 same value of $\langle v = 0 | \mu(\text{CO}_2) | v_3 = 1 \rangle$ [42,43], but a change of the ν_3 band origin from 2349 to 2283
 259 cm⁻¹.

260

261 4. Results and discussion

262 As said above, the ¹²CO₂ and ¹³CO₂ CIA bands as obtained from experiments were fitted assuming
 263 a Lorentzian band shape (see **Figs. 1** and **3**). In the case of the main isotopologue, the underlying far
 264 wing continuum was fixed to its value calculated by the χ -factor approach (see [11]). In the case of
 265 ¹³CO₂, the baseline was assumed to be constant with frequency and it was adjusted by the fit. The
 266 CMDS-computed spectra for ¹²CO₂ and ¹³CO₂ were fitted by a Gaussian function to determine the
 267 center position, their integration over wavenumber yielded the intensities, and the widths were

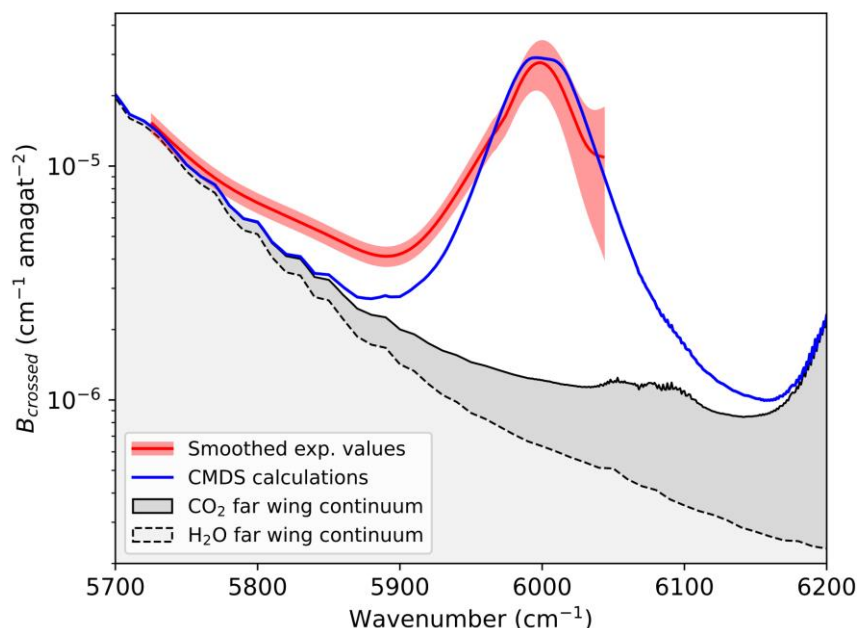
268 determined directly from the computed absorptions. The experimental and calculated centers,
 269 integrated areas and half-widths at half-maximum (HWHM) are listed in **Table 1**, calling for several
 270 remarks. The first is that the peak positions obtained for the measured spectra and from those
 271 computed using CMDS (corrected as explained in Sec. 3 to take the H₂O Q lines true quantum positions
 272 into account) agree very well. The measured and calculated differences between the ¹²CO₂ and ¹³CO₂
 273 values, of about 68 cm⁻¹, are in close agreement with the isotopic shift of the $\nu_3 = 1$ vibrational levels
 274 of the two isotopologues (66 cm⁻¹) [44]. The second is that the measured and computed integrated
 275 intensities also coincide, with differences well smaller than the experimental uncertainty (roughly
 276 estimated to 20 % and 30 % for ¹²CO₂ and ¹³CO₂, respectively). The integrated band intensities for the
 277 two isotopologues are close, as could be expected from the fact that the CO₂ dipole matrix elements
 278 are practically identical [42,43]. Finally, the experimental and predicted HWHM are again consistent,
 279 both showing a negligible isotope effect, as could be expected from the strong similarity between ¹²CO₂
 280 and ¹³CO₂.

	$\nu_3(^{12}\text{CO}_2)+\nu_1(\text{H}_2\text{O})$		$\nu_3(^{13}\text{CO}_2)+\nu_1(\text{H}_2\text{O})$	
	Exp	CMDS	Exp	CMDS
Center (cm ⁻¹)	5998.4	5999.7	5930.2	5932
Integrated binary coefficient (10 ⁻³ cm ⁻² amagat ⁻²)	2.6	2.08	2.1	2.06
HWHM (cm ⁻¹)	33.0	31	28.2	31

281
 282 **Table 1:** Band centers, integrated intensities and half widths at half maximum (HWHM) of the $\nu_3(\text{CO}_2)+\nu_1(\text{H}_2\text{O})$
 283 CIA bands measured and CMDS-calculated for natural ¹²CO₂ and in ¹³CO₂.
 284

285 A comparison between the measured and computed H₂O-¹²CO₂ density-normalized absorption
 286 coefficients over the spectral range of the 1.6 μm window is displayed in **Fig. 4**. The calculated
 287 spectrum was obtained by adding the CIA predicted in the present study to the contributions of the
 288 far wings of the H₂O-broadened transitions of CO₂ and of the CO₂-broadened lines of H₂O. The
 289 associated values of the binary coefficients, $B_{\text{CO}_2-\text{H}_2\text{O}}$ and $B_{\text{H}_2\text{O}-\text{CO}_2}$, were calculated with the χ -factor
 290 approaches developed in Refs. [8] and [9] respectively. As can be seen, the agreement is quite
 291 satisfactory which validates the prediction of all three contributions. However there is a noticeable
 292 discrepancy between measured and computed values on the low frequency side of the CIA peak which
 293 may be explained by the neglecting of the contribution of the anisotropic polarizability $\Delta\alpha$ of H₂O in
 294 the CMDS computation of the collision-induced dipole. Indeed, first note that, since $\langle v = 0 | \Delta\alpha(\text{H}_2\text{O}) | v_1 = 1 \rangle = 0.54$ a. u. (obtained from the value of α_0^2 provided in Ref. [40] and $\Delta\alpha =$
 295 $\sqrt{3/2} \alpha_0^2$) which is smaller than $\langle v = 0 | \alpha_{iso}(\text{H}_2\text{O}) | v_1 = 1 \rangle = 0.73$ a. u. by a factor of about $\sqrt{2}$, the
 296 integrated intensity due to this dipole induction mechanism should be about 2 times lower. In addition,
 297 the anisotropic polarizability selection rule allows not only Q but also O and S lines associated with J
 298 $\rightarrow J \pm 2$ transitions, the latter being spread over a broad spectral range of several 100 cm⁻¹ on both sides
 299

300 of the central vibrational frequency. In summary, this contribution, which is weaker and spectrally
 301 much broader than that of the isotropic polarizability, may explain the above mentioned missing
 302 "background".



303
 304 **Fig 4:** Crossed binary coefficients in the region of the $\nu_3(^{12}\text{CO}_2)+\nu_1(\text{H}_2\text{O})$ CIA band. The CIA predicted by CMDS
 305 calculations (blue) is added to the sum of the H₂O (light grey) and CO₂ (grey) far wing continua. Also shown are
 306 the smoothed experimental values from Ref. [11] (red, with a 1σ error band).
 307

308 It is worth mentioning that the $\nu_3(\text{CO}_2)+\nu_1(\text{H}_2\text{O})$ CIA band presently measured in the gas phase
 309 at sub-atmospheric pressure was pointed out nearly three decades ago in liquid CO₂+H₂O mixtures,
 310 thus at considerably higher molecular densities [10]. Low resolution spectra were recorded with
 311 grating spectrographs allowing for an estimation of the integrated absorption cross-section. A value of
 312 $8\times 10^{-4} \text{ cm}^{-2}\text{amagat}^{-2}$ was estimated in the liquid phase, about three times smaller than our gas phase
 313 value ($2.6\times 10^{-3} \text{ cm}^{-2}\text{amagat}^{-2}$). Note that a similar tendency between liquid and gas phase CIA
 314 intensities (normalized to squared density) was reported for the far-infrared CIA of pure CO₂ [45]. Let
 315 us also mention that the simultaneous CO₂-H₂O transitions investigated in the present study have many
 316 points in common with those of CO₂-H₂ observed and analyzed more than sixty years ago in [24].
 317 Indeed, both involve the ν_3 CO₂ dipole and a vibrational change of the other molecule through the
 318 polarizability.

319 In general, free collisions are believed to bring most of the contribution to CIA bands, except at
 320 (very) low temperature, while H₂O-CO₂ bound complexes, which are disregarded in the CMDS, are not
 321 expected to contribute significantly to the observed absorption feature. This seems reasonable at the
 322 room temperature of this study considering the expected very small portion of bound dimers. The
 323 agreement between the measured and CMDS integrated band intensities seems to confirm this

324 expectation. The H₂O-CO₂ bound complex which has been observed in matrices (e.g. [46]) and in
 325 expansion jets (e.g. [47,48]) has a planar T-shaped structure with hydrogens pointing away from CO₂.
 326 The dissociation energy D_0 was estimated to be about 730 cm⁻¹ [49,50]. It is worth mentioning the
 327 results of anharmonic vibrational calculations of the spectrum of this Van der Waals complex [51],
 328 based on *ab initio* force field and electro-optical parameters. As expected, most of the predicted
 329 vibrational bands of the H₂O-CO₂ complex fall in coincidence with those of pure H₂O or CO₂ but,
 330 interestingly, Pavlyuchko et al. concluded their article by noting that "...the combination
 331 transition $\nu_{OH}^S + \nu_{CO}^{AS}$ [e.g. $\nu_3(\text{CO}_2) + \nu_1(\text{H}_2\text{O})$] in the vicinity of ~ 6000 cm⁻¹, falls occasionally in the
 332 regions of relative transparency of both isolated monomers and can therefore be discriminated from
 333 the monomer absorption" [51]. Although our observation cannot be interpreted as an absorption band
 334 of the H₂O-CO₂ bound complex, the above statement about the detection of simultaneous transitions
 335 applies to the CIA in (H₂O+CO₂) gas mixtures.

336 5. Conclusion

337 The present study, thanks to measurements and classical molecular dynamics calculations made
 338 for both ¹²CO₂-H₂O and ¹³CO₂-H₂O mixtures, has confirmed that the band observed around 6000 cm⁻¹
 339 in Ref. [11] is indeed due to the dipole induced in interacting (CO₂, H₂O) pairs through the
 340 $\nu_3(\text{CO}_2) + \nu_1(\text{H}_2\text{O})$ simultaneous transitions, involving a $\Delta\nu_3 = 1$ change of CO₂ through the dipole and a
 341 $\Delta\nu_1 = 1$ change of H₂O through the polarizability. It is worth emphasizing that this is the first
 342 demonstration of a purely collision-induced absorption contribution to the binary continuum in CO₂ +
 343 H₂O gas mixtures, which was so far entirely attributed to the far line wings of the dipole transitions of
 344 CO₂ broadened by H₂O and of H₂O broadened by CO₂.

345 Note that other simultaneous transitions in H₂O+CO₂ gas mixtures exist which may be
 346 detectable, since centered in some relatively transparent regions of the H₂O+CO₂ spectrum, and thus
 347 deserve investigation. The first [$\nu_3(\text{CO}_2) + \nu_3(\text{H}_2\text{O})$] is similar to the one studied in this paper, but in which
 348 a H₂O ν_3 Raman vibrational change is involved, which would lead to a CIA centered around 6105 cm⁻¹.
 349 This CIA is expected to be small and broad, since $\langle v = 0 | \alpha_{iso}(\text{H}_2\text{O}) | v_3 = 1 \rangle = 0$ [40] and thus only
 350 the $\langle v = 0 | \Delta\alpha(\text{H}_2\text{O}) | v_3 = 1 \rangle$ matrix element contributes. Another contribution comes from the
 351 $\nu_2(\text{CO}_2) + \nu_1(\text{H}_2\text{O})$ transition, involving, among others, the contributions of the products $\langle v =$
 352 $0 | \Delta\alpha(\text{H}_2\text{O})$ and $\alpha_{iso}(\text{H}_2\text{O}) | v_1 = 1 \rangle \langle v = 0 | \mu(\text{CO}_2) | v_2 = 1 \rangle$, which for ¹²CO₂ should peak near 4334
 353 cm⁻¹. The associated CIA band is expected to be less intense than the one investigated in this study due
 354 to the smaller central wavenumber and weaker CO₂ dipole matrix element ($\langle v = 0 | \mu(\text{CO}_2) | v_2 = 1 \rangle =$
 355 0.071 a.u. [38,39]). For completeness, note that two other simultaneous transitions should appear
 356 around 2900 cm⁻¹, $\nu_1(\text{CO}_2) + \nu_2(\text{H}_2\text{O})$ and $2\nu_2(\text{CO}_2) + \nu_2(\text{H}_2\text{O})$, associated with the polarization of CO₂ by
 357 the dipole of H₂O, through the product $\langle v = 0 | \Delta\alpha(\text{CO}_2)$ and $\alpha_{iso}(\text{CO}_2) | v_1 = 1$ or $v_2 = 2 \rangle \langle v =$
 358 $0 | \mu(\text{H}_2\text{O}) | v_2 = 1 \rangle$.

359

360 **Acknowledgements**

361 This work was performed in the frame of the ANR project COMPLEAT (ANR-19-CE31-0010-01). H. Tran
362 and M. Turbet (LMD) are thanked for providing the $B_{CO_2-H_2O}$ and $B_{H_2O-CO_2}$ binary coefficients
363 calculated with the χ -factor approach. AC is grateful to Andrey Vigasin for useful exchanges. WF and J-
364 MH thank Prof. Christian Boulet for very helpful discussions.

References

- 365
366
367 [1] Hartmann J-M, Tran H, Armante R, Boulet C, Campargue A, Forget F, Gianfrani L, Gordon I, Guerlet S,
368 Gustafsson M, Hodges JT, Kassi S, Lisak D, Thibault F, Toon GC. Recent advances in collisional effect on spectra
369 of molecular gases and their practical consequences. *J Quant Spectrosc Radiat Transf* 2018;213:178–227.
370 doi:10.1016/j.jqsrt.2018.03.016.
- 371 [2] Hartmann J-M, Boulet C, Robert D. Collisional effects on molecular spectra: laboratory experiments and
372 models, consequences for applications. Elsevier; 2021. Second Edition Amsterdam.
- 373 [3] Hartmann J-M, Boulet C, Tran DD, Tran H, Baranov Y. Effect of humidity on the absorption continua of CO₂
374 and N₂ near 4 μm: Calculations, comparisons with measurements, and consequences for atmospheric spectra.
375 *J Chem Phys* 2018;148:054304. doi:10.1063/1.5019994.
- 376 [4] Hartmann J-M, Armante R, Toon GC, Scott N, Tran H, Crevoisier C, Chédin A, Capelle V. Indirect influence of
377 humidity on atmospheric spectra near 4 μm. *Geophys Res Lett* 2018;45:12593–12601.
378 doi:10.1029/2018GL079582.
- 379 [5] Ma Q, Tipping RH. A far wing line shape theory and its application to the foreign-broadened water continuum
380 absorption. III. *J Chem Phys* 1992;97:818–828. doi:10.1063/1.463184.
- 381 [6] Pollack JB, Dalton JB, Grinspoon D, Wattson RB, Freedman R, Crisp D, Allen DA, Bézard B, DeBergh C, Giver
382 LP, Ma Q, Tipping RH. Near-Infrared Light from Venus' Nightside: A Spectroscopic Analysis. *Icarus* 1993;103:1–
383 42. doi:10.1006/icar.1993.1055.
- 384 [7] Baranov YI. On the significant enhancement of the continuum-collision induced absorption in H₂O+CO₂
385 mixtures. *J Quant Spectrosc Radiat Transf* 2016;175:100–6. doi:10.1016/j.jqsrt.2016.02.017.
- 386 [8] Tran H, Turbet M, Chelin P, Landsheere X. Measurements and modeling of absorption by CO₂+H₂O mixtures
387 in the spectral region beyond the CO₂ v₃-band head. *Icarus* 2018;306:116–121.
388 doi:10.1016/j.icarus.2018.02.009.
- 389 [9] Tran H, Turbet M, Hanoufa S, Landsheere X, Chelin P, Ma Q, Hartmann J-M. The CO₂-broadened H₂O
390 continuum in the 100–1500 cm⁻¹ region: Measurements, predictions and empirical model. *J Quant Spectrosc*
391 *Radiat Transf* 2019;230:75–80. doi:10.1016/j.jqsrt.2019.03.016.
- 392 [10] Vigasin AA, Adiks TG, Tarakanova EG, Yuxhnevich GV. Simultaneous infrared absorption in a mixture of CO₂
393 and H₂O: The role of hydrogen-bonded aggregates. *J Quant Spectrosc Radiat Transf* 1994;52:295-301.
394 doi:10.1016/0022-4073(94)90159-7.
- 395 [11] Fleurbaey H, Campargue A, Carreira Mendès da Silva Y, Grilli R, Kassi S, Mondelain D. Characterization of the
396 foreign water vapor continuum in CO₂ within the infrared transparency windows. *J Quant Spectrosc Radiat*
397 *Transf* 2022; 282 108119 doi.org/10.1016/j.jqsrt.2022.108119
- 398 [12] Mondelain D, Campargue A, Čermák P, Gamache RR, Kassi S, Tashkun SA, Tran H. The CO₂ absorption
399 continuum by high pressure CRDS in the 1.74 μm window. *J Quant Spectrosc Radiat Transfer* 2017;203:530–
400 537. doi:10.1016/j.jqsrt.2017.02.019.
- 401 [13] Welsh HL, Crawford MF, MacDonald JCF, Chisholm DA. Induced Infrared Absorptions of H₂, N₂, and O₂ in the
402 First Overtone Regions. *Phys Rev* 1951;83:1264-64. doi:10.1103/PhysRev.83.1264.
- 403 [14] Brodbeck C, Bouanich J-P, Figuiere P, Szwarc H. Simultaneous infrared transitions in N₂ + SF₆ mixtures. *J*
404 *Chem Phys* 1981;74:77–80. doi:10.1063/1.440796.
- 405 [15] Bouanich J-P, Brodbeck C. Collision-induced simultaneous transitions in H₂+CF₄ and H₂+SF₆ mixtures. *J Quant*
406 *Spectrosc Radiat Transf* 1977;17:777–82. doi:10.1016/0022-4073(77)90045-3.
- 407 [16] Abu-Kharma M. Analysis of the collision-induced absorption spectra of H₂ in H₂-N₂ in the range 5600–9500
408 cm⁻¹. *J Phys B: At Mol Opt Phys* 2007;40:2345–50. doi:10.1088/0953-4075/40/12/010.
- 409 [17] Stamp S, Prasad RDG, Gillard PG, Paddi Reddy S. Analysis of the collision-induced absorption spectra of
410 double vibrational transitions in H₂-N₂", *AIP Conference Proceedings* 1999;467:453–456.
411 doi:10.1063/1.58384.

- 412 [18] Tonkov MV, Filippov NN, Bertsev VV, Bouanich JP, Nguyen Van Thanh, Brodbeck C, et al. Measurements and
413 empirical modelling of pure CO₂ absorption in the 2.3 μm region at room temperature: far wings, allowed
414 and collision-induced bands. *Appl Opt* 1996;35:4863–70. doi:10.1364/AO.35.004863.
- 415 [19] Fahrenfort J, Ketelaar JAA. Simultaneous Vibrational Transitions in the Infrared Absorption Spectra of
416 Compressed Gases. *J Chem Phys* 1954;22:1631. doi:10.1063/1.1740502.
- 417 [20] Keteelar JAA. Infra-red spectra of compressed gases. *Spectrochim Acta* 1959;14:237–248. doi:10.1016/0371-
418 1951(59)80231-9.
- 419 [21] Brodbeck C, Bouanich J-P, Penner AR, Meinander N, Tabisz GC. Band-shape analysis of an infrared double
420 transition in CO₂ + N₂ gas mixtures. *Can J Phys* 1987;65:1073–1076. doi:10.1139/p87-177.
- 421 [22] Maté B, Fraser GT, Lafferty WJ. Intensity of the simultaneous vibrational absorption CO₂ (ν₃=1) + N₂ (ν=1) ←
422 CO₂ (ν₃=0) + N₂ (ν=0) at 4680 cm⁻¹. *J Mol Spectrosc* 2000;201:175–177. doi:10.1006/jmsp.2000.8074.
- 423 [23] Brown A, Tipping RH, Maté B. Theoretical Study of the Collision-Induced Double Transition CO₂ (ν₃=1) + N₂
424 (ν₁=1) ← CO₂ (ν₃=0) + N₂ (ν₁=0) at 296 K. *J Mol Spectrosc* 2000;204(1):153–158. doi:10.1006/jmsp.2000.8214.
- 425 [24] Colpa JP, Ketelaar JAA. The absorption intensity of simultaneous vibrational transitions in gas mixtures.
426 *Physica* 1958;24:1035-44. doi:10.1016/S0031-8914(58)80122-6.
- 427 [25] Kassi S, Campargue A, Mondelain D, Tran H. High pressure Cavity Ring Down Spectroscopy: Application to
428 the absorption continuum of CO₂ near 1.7 μm. *J Quant Spectrosc Radiat Transf* 2015;167:97–104.
429 doi:10.1016/j.jqsrt.2015.08.014.
- 430 [26] Campargue A, Kassi S, Mondelain D, Vasilchenko S, Romanini D. Accurate laboratory determination of the
431 near infrared water vapor self-continuum: A test of the MT_CKD model. *J Geophys Res Atmos*
432 2016;121:13180–13203. doi:10.1002/2016JD025531.
- 433 [27] Lechevallier L, Vasilchenko S, Grilli R, Mondelain D, Romanini D, Campargue A. The water vapour self-
434 continuum absorption in the infrared atmospheric windows: new laser measurements near 3.3 and 2.0 μm.
435 *Atmos Meas Tech* 2018;11:2159–2171. doi:10.5194/amt-11-2159-2018.
- 436 [28] Richard L, Vasilchenko S, Mondelain D, Ventrillard I, Romanini D, Campargue A. Water vapor self-continuum
437 absorption measurements in the 4.0 and 2.1 μm transparency windows. *J Quant Spectrosc Radiat Transf*
438 2017;201:171–179. doi:10.1016/j.jqsrt.2017.06.037.
- 439 [29] Ventrillard I, Romanini D, Mondelain D, Campargue A. Accurate measurements and temperature
440 dependence of the water vapor self-continuum absorption in the 2.1 μm atmospheric window. *J Chem Phys*
441 2015;143:134304. doi:10.1063/1.4931811.
- 442 [30] Vasilchenko S, Campargue A, Kassi S, Mondelain D. The water vapour self- and foreign-continua in the 1.6
443 μm and 2.3 μm windows by CRDS at room temperature. *J Quant Spectrosc Radiat Transf* 2019;227:230–238.
444 doi:10.1016/j.jqsrt.2019.02.016.
- 445 [31] Fleurbaey H, Grilli R, Mondelain D, Campargue A. Measurements of the water vapor continuum absorption
446 by OFCEAS at 3.50 μm and 2.32 μm. *J Quant Spectrosc Radiat Transf* 2022;278:108004.
447 doi:10.1016/j.jqsrt.2021.108004.
- 448 [32] Fleurbaey H, Reed ZD, Adkins EM, Long DA, Hodges JT. High accuracy spectroscopic parameters of the 1.27
449 μm band of O₂ measured with comb-referenced, cavity ring-down spectroscopy. *J Quant Spectrosc Radiat*
450 *Transf* 2021;270:107684. doi:10.1016/j.jqsrt.2021.107684.
- 451 [33] Mondelain D, Kassi S, Campargue A. Accurate laboratory measurement of the O₂ collision-induced
452 absorption band near 1.27 μm. *J Geophys Res: Atmospheres* 2019;124:414–423. doi:10.1029/2018JD029317.
- 453 [34] Kassi S, Guessoum S, Abanto JCA, Tran H, Campargue A, Mondelain D. Temperature dependence of the
454 collision-induced absorption band of O₂ near 1.27 μm. *J Geophys Res: Atmospheres*
455 2021;126:e2021JD034860. doi:10.1029/2021JD034860.
- 456 [35] Gordon IE, Rothman LS, Hill C, Kochanov RV, Tan Y, Bernath PF, Birk M, Boudon V, Campargue A, et al. The
457 HITRAN2016 Molecular Spectroscopic Database. *J Quant Spectrosc Radiat Transf* 2017;203:3–69.
458 doi:10.1016/j.jqsrt.2017.06.038.
- 459 [36] Allen MP, Tildesley DJ. *Computer simulations of liquids*. Oxford University Press 1987, Oxford.
- 460 [37] Frommhold L. *Collision Induced Absorption in Gases*. Cambridge Monographs on Atomic, Molecular, and
461 *Chemical Physics*. Cambridge University Press 2006, Cambridge.

- 462 [38] Kolomiitsova TD, Lyaptsev AV, Shchepkin DN. Determination of parameters of the dipole moment of the CO₂
463 molecule. *Opt Spectrosc* 2000;88:648–60. doi:10.1134/1.626856.
- 464 [39] Liang Z, Tsai HL. Determination of vibrational energy levels and transition dipole moments of CO₂ molecules
465 by density functional theory. *J Mol Spectrosc* 2008;252:108–14. doi:10.1016/j.jms.2008.07.008.
- 466 [40] Avila G, Fernández JM, Tejada G, Montero S. The Raman spectra and cross-sections of H₂O, D₂O, and HDO in
467 the OH/OD stretching regions. *J Mol Spectrosc* 2004;228:38–65. doi:10.1016/j.jms.2004.06.012.
- 468 [41] Hartmann JM, Boulet C, Jacquemart D. Molecular dynamics simulations for CO₂ spectra. II. The far infrared
469 collision-induced absorption band. *J Chem Phys* 2011; 134:094316. doi:10.1063/1.3557681.
- 470 [42] Johns JWC. Absolute intensities in CO₂: The 4.3- and 2.7- μ m regions revisited. *J Mol Spectrosc* 1989;134:433-
471 9. doi:10.1016/0022-2852(89)90328-7.
- 472 [43] Gordon IE, Rothman LS, Hargreaves RJ, Hashemi R, Karlovets EV, Skinner FM, Conway EK, Hill C, et al. The
473 HITRAN2020 Molecular Spectroscopic Database. *J Quant Spectrosc Radiat Transf* 2022;277:107949.
474 doi:10.1016/j.jqsrt.2021.107949.
- 475 [44] Rothman LS, Hawkins RL, Wattson RB, Gamache RR. Energy levels, intensities, and linewidths of atmospheric
476 carbon dioxide bands. *J Quant Spectrosc Radiat Transf* 1992;48:537–66. doi:10.1016/0022-4073(92)90119-
477 O.
- 478 [45] Ho W, Birnbaum G, Rosenberg A. Far-infrared collision-induced absorption in CO₂. I. Temperature
479 dependence. *J Chem Phys* 1971;55:1028. doi:10.1063/1.1676181
- 480 [46] Schriver A, Schriver-Mazzuoli L, Chaquin P, Dumont E. FTIR and ab Initio Study of the 1/1 Complex between
481 Water and Carbon Dioxide in Solid Nitrogen. *J Phys Chem A* 2006;110:51–56. doi:10.1021/jp0581328.
- 482 [47] Zhu Y, Li S, Sun P, Duan C. Infrared diode laser spectroscopy of H₂O–CO₂ and D₂O–CO₂ complexes in the ν_2
483 bend region of water. *J Mol Spectrosc* 2013;283:7–9. doi:10.1016/j.jms.2012.12.002.
- 484 [48] Bogomolov AS, Roucou A, Bejjani R, Herman M, Moazzen-Ahmadi N, Lauzin C. The rotationally resolved
485 symmetric 2OH excitation in H₂O–CO₂ observed using pulsed supersonic expansion and CW-CRDS. *Chem Phys*
486 *Letters* 2021;774:138606. doi:10.1016/j.cplett.2021.138606.
- 487 [49] Makarewicz J. Intermolecular potential energy surface of the water-carbon dioxide complex. *J Chem Phys*
488 2010;132:234305. doi:10.1063/1.3439693.
- 489 [50] Andersen J, Heimdal J, Mahler DW, Nelander B, Wugt Larsen R, et al. Communication: THz absorption
490 spectrum of the CO₂–H₂O complex: Observation and assignment of intermolecular van der Waals vibrations.
491 *J Chem Phys* 2014;140:091103. doi:10.1063/1.4867901.
- 492 [51] Pavlyuchko AI, Orlinson BS, Viganin AA. Variational Solution of Anharmonic Vibrational Problems for
493 Polyatomics and Molecular Pairs. In: Camy-Peyret C, Viganin AA (eds) *Weakly Interacting Molecular Pairs:*
494 *Unconventional Absorbers of Radiation in the Atmosphere.* NATO Science Series (Series IV: Earth and
495 Environmental Sciences), vol 27. Springer, Dordrecht. 2003, pp. 73–82. doi:10.1007/978-94-010-0025-3_5.
- 496
- 497